The Cryosphere Discuss., 6, 3613–3646, 2012
www.the-cryosphere-discuss.net/6/3613/2012/
doi:10.5194/tcd-6-3613-2012

The Cryosphere Discussions

Mapping radiation transfer through sea ice using a remotely operated vehicle (ROV)

M. Nicolaus and C. Katlein

Alfred Wegener Institute for Polar and Marine Research, Bremerhaven, Germany

Received: 8 August 2012 – Accepted: 14 August 2012 – Published: 3 September 2012

Correspondence to: M. Nicolaus (marcel.nicolaus@awi.de)

Published by Copernicus Publications on behalf of the European Geosciences Union.

Abstract

Light (solar short-wave radiation) transmission into and through sea ice is of high importance for various processes in Polar Regions. The amount of energy transferred through the ice determines formation and melt of sea ice and finally contributes to warming of the uppermost ocean. At the same time the amount and distribution of light, as the primary source of energy, is of critical importance for sea-ice associated organisms and bio-geochemical processes. However, our current understanding of these processes and their interdisciplinary interactions is still sparse. The main reason is that the under-ice environment is difficult to access and measurements require large logistical and instrumental efforts. Particularly, it was not possible to map light conditions under sea ice over larger areas. Here we present a detailed methodical description of operating spectral radiometers on a remotely operated vehicle (ROV) in the Central Arctic under sea ice. This new measurement concept resulted in a most comprehensive data set of spectral radiance and irradiance under and above sea ice, complemented through various additional in-situ measurements of sea-ice, snow, and surface properties. Finally, such data sets allow quantifying the spatial variability of light under sea ice, especially highlighting differences between ponded and white ice as well as different ice types.

1 Introduction

The amount of solar short-wave radiation (sun light) reflected to the atmosphere (albedo), absorbed by snow and sea ice, and transmitted into the upper ocean (transmittance) is of critical importance for the energy budget of sea-ice covered seas. In particular, these determine the formation and melt of sea ice, as well as snow metamorphism and melt. In addition, the amount of light in and under sea ice is of critical importance for biological processes (e.g. primary productivity) and biogeochemical fluxes (Popova et al., 2012; Deal et al., 2011; Arrigo et al., 2012). Nevertheless, energy

TCD
6, 3613–3646, 2012

fluxes through snow and sea ice are still not well quantified, even though Perovich (2005) demonstrated their importance, estimating that light penetration through bare and ponded sea ice amounts to 16 and 23 % of surface irradiance, respectively.

From various observations, it is known that physical properties and thickness of snow and sea-ice are highly variable (e.g. Warren et al., 1999; Sturm and Massom, 2009). This holds for temporal variability from diurnal to seasonal cycles as well as for spatial variability on scales from meters to hundreds of kilometers. As a consequence of this high variability, light transmittance through snow and sea ice is also expected to be most variable (e.g. Perovich, 1990; Grenfell et al., 2006; Mundy et al., 2005; Light et al., 2008), resulting in large differences in the horizontal and vertical distribution of sun light in sea ice and the uppermost ocean.

In addition to changes in the total amount of transmitted solar irradiance, the spectral composition also varies as a function of snow, sea-ice, and water properties (Perovich, 1996; Light et al., 2008), as well as through the abundance of biota and sediments (Ficek et al., 2004; Mundy et al., 2007). All these components have specific absorption spectra, impacting spectral radiation in and under sea ice. Based on this, Perovich et al. (1993) and later, in more detail, Mundy et al. (2007) derived methods to estimate under-ice biomass based on optical measurements.

During the last years, the number of studies of spectral light measurements under sea ice has increased. Using classical spot measurements, Ehn et al. (2011) quantified the horizontal spreading of light in ponded sea ice, and Frey et al. (2011) described the vertical distribution of light under pond-covered sea ice. The most comprehensive study of seasonal variability of light transmittance through sea ice was presented by Nicolaus et al. (2010a), using a stationary setup on drifting multi-year ice in the Arctic (Nicolaus et al., 2010b).

However, observations that provide insights into the spatial variability of under-ice irradiance and radiance are still sparse, and little is known about how light conditions change at different scales. The first remotely operated vehicle (ROV) based measurements of under-ice irradiance were performed by Perovich et al. (1998) on land-fast

TCD
6, 3613–3646, 2012

sea ice off the coast of Barrow, Alaska, in April 1996. Recently, Nicolaus et al. (2012) investigated the spatial variability of optical properties of land-fast sea ice in a very similar way, but including repetitions of the transect throughout the melt season.

In order to describe the spatial variability of different types of drifting Arctic sea ice, we have operated spectral radiometers on a ROV during a cruise to the Central Arctic in summer 2011. Here we describe methods and results of irradiance and radiance measurements based on horizontal and vertical transects. The measurements were performed under ponded and white first-year ice (FYI) and multi year ice (MYI), as well as under new sea ice (frozen lead) and in open water. The ROV was operated directly from the sea ice in order to be least influenced by the vessel and to allow additional measurements along the transects. In the end, comprehensive data set of light conditions under very different ice regimes was collected, revealing new insights into the horizontal and vertical distribution of spectral solar radiation under sea ice.

2 Methods

2.1 Measurements during a trans-polar expedition

All measurements were performed during the cruise ARK-XXVI/3 (TransArc) of the German icebreaker F/S *Polarstern* into the Central Arctic Ocean from 4 August to 7 October 2011. As illustrated in Fig. 1, a large transect across the Arctic Ocean was performed, entering the sea ice north of Franz Josef Land, crossing the North Pole into the Canadian Basin, and returning via the Russian Shelf regions. With this, the horizontal and vertical distributions of solar radiation under sea ice were measured in different regions of the Central Arctic during summer. Sea-ice and surface conditions varied along the cruise track: FYI and open melt ponds dominated the first part of the cruise. Starting from the North Pole station on 22 August 2012, larger fractions of MYI were observed and sampled (stations on 22 August, 3 and 16 September). Surface conditions then also changed from open ponds and wet surfaces to frozen and even

TCD
6, 3613–3646, 2012

snow covered surfaces towards the end of the cruise (Table 1). Since the cruise track reached into the Canadian Basin, the stations on 3 and 6 September were dominated by Pacific waters under the sea ice, in contrast to dominating Atlantic waters at the other stations.

One focus of the sea-ice physics program during the cruise was to conduct ROV-based measurements of spectral irradiance and radiance under sea ice. The aim of these measurements was to quantify the spatial variability of radiation fluxes under sea ice. Successful measurements were performed during 9 ice stations (Fig. 4), covering ponded and white FYI and MYI, new sea ice (frozen lead), and open water. In addition to the optical measurements, a comprehensive data set of sea-ice, surface, and snow properties were recorded, in order to classify the optical data and enable developments of parameterizations for radiation fluxes through different ice types. Station duration was mostly about 8 h, except one 36-h station at the North Pole. Furthermore, stationary optical measurements were performed coincident to sea ice core extractions, but these measurements and data are not included here.

2.2 ROV instrumentation

A V8ii ROV (Ocean Modules, Åtvidaberg, Sweden) was used as the sensor platform. This ROV type was selected because of its size, power, freedom of movement, and good experiences during an Antarctic expedition (personal communication, 2011; K. Meiners, Antarctic CRC, data unpublished). A main requirement was the possibility to handle it with only two persons on the sea ice and launch and recover it through holes smaller than 1.0 m^2. The main instruments on board (pay load) were two spectral radiometers (see below).

The ROV system consisted of a surface unit (incl. power supply, control unit, monitor), a 300-m tether cable, and the ROV itself. The ROV is controlled and moved by eight thrusters allowing a diving speed of up to 1.0 $m\,s^{-1}$. The standard measurement speed (using 25 % thruster gain) was about 0.25 $m\,s^{-1}$ for horizontal and vertical profiles. The speed varied from profile to profile and depended on under-ice currents as

TCD
6, 3613–3646, 2012

well. The ROV was equipped with two VGA video cameras, one zoom-camera looking forward (Typhoon, Tritech, Aberdeen, UK) and one with a fixed focal length looking backward (Ospray, Tritech, Aberdeen, UK) (Fig. 2). Both cameras were used for navigation (orientation) and to document the dives. The video signal of the forward-looking camera was recorded continuously. An altimeter (DST Micron Echosounder, Tritech, Aberdeen, UK) and a sonar (Micron DST MK2, Tritech, Aberdeen, UK) were mounted to support navigation and measure the distances to obstacles and markers (see below). The altimeter was particularly used to measure the distance between the ROV (finally also the radiometers) and the sea-ice bottom. In addition, the ROV measured its depth, heading, roll, pitch, and turns and displayed this as an overlay together with a time stamp on the control monitor (Fig. 5).

2.3 ROV operation

The ROV can be powered with a 5-kW generator. But due to a failure of the generator, ship's power had to be used for all measurements. For this, 100 to 150 m of extension cords had to be laid out from the vessel to the ROV site. This limited the choice of the launch site to a distance smaller than the cable length, but still far enough to avoid any shadows and obvious influences of the vessel. The ROV was balanced in a pool on the working deck of R/V *Polarstern* with Arctic seawater. Differently from standard ROV applications, the ROV and the tether were trimmed slightly heavy for the under-ice operations in order to sink in case of failure. Thus it would be hanging straight under the launch hole and could be pulled up again. Salinity variations between the stations, due to sea ice melt, led to slight variations in balancing throughout the cruise, but did not significantly influence the ROV navigation and handling.

All electronics were set up in a pilot tent (Fig. 3), which was heated when necessary. Flying the ROV was most efficient with four persons: one pilot controlling the ROV, one co-pilot controlling the optical sensors and documenting the dive, one person to handle the tether, and one designated polar-bear guard. The ROV was mostly launched through melt ponds, which were melted (almost) all the way through (Fig. 4). On 16

TCD
6, 3613–3646, 2012

September, no such pond was present and the ROV was launched over the floe edge at a sheltered location, reducing the risk that drifting ice could block the launch site. These procedures worked out nicely and reduced the amount of work for access-hole preparation to a minimum, at least under the given summer conditions. After an initial system check and a local test survey to judge the under-ice conditions (visibility, currents, under-ice topography), transects (grids) were marked with numbered, red-white colored poles, hanging under the ice through drill holes (Fig. 5). Marker positions were measured with measuring tape or a handheld GPS receiver and corrected for sea-ice drift. The under-ice markers were of critical importance for under-ice orientation, since a designated navigation system was not available for this cruise. For depth profiles (green arrows in Fig. 4), a rope with a weight was lowered through a borehole. Firmly following this rope helped to keep the horizontal position during descent and ascent, as accurate as possible.

The preferred mode of operation for the ROV is "normal horizon". In this mode, the ROV stabilizes and keeps its position and orientation in the water automatically, except for displacements by currents. This mode was used on the first two ROV ice-stations (until 22 August) without any problems. Closer to the magnetic (south) pole (approx. at 137.3° W and 85.25° N) "normal horizon" could not be used, because stabilization requires a stable compass reading, which was not given in areas where the horizontal component of the magnetic field strength was below 2000 nT. Alternatively, the ROV was flown in "deck mode", without any automatic stabilization, but no useful data were recorded since no stable ROV positioning could be achieved (31 August). From 3 September onwards, the magnetic field was again strong enough to prevent the ROV from uncontrolled movements. The ROV was flown in "VG horizon" (a driving mode stabilized by a gyro-compass) or "normal horizon" again. However, due to a strong compass and gyro drift, the heading information could not be used for navigation any more and more manual adjustments were necessary. Overall, 6 to 8 h were needed for the ROV work, including setup, deployment of under-ice markers, optical and additional measurements, and packing.

TCD
6, 3613–3646, 2012

2.4 Spectral radiation measurements

Spectral radiance and irradiance in the wavelength range from 350 to 920 nm (3.3 nm resolution) were measured with Ramses spectral radiometers (Trios GmbH, Rastede, Germany). Technical details about the sensors and data processing are described in Nicolaus et al. (2010b). Under-ice radiance ($I_{d,u}$, 7° field of view) was mainly measured to study the spatial variability of optical properties of sea ice, because the measured signal originates from a comparably small area. Under-ice irradiance ($E_{d,u}$, cosine receptor) was mainly measured to study the energy budget at the point of measurement, integrating all incident energy (from above) at this point. The $E_{d,u}$ sensor (type SAMIP) was directly implemented into the ROV, meaning its communication was led through the tether, using the last available twisted pair. The $I_{d,u}$ sensor (type SAM) was connected through a separate 150-m long cable, which was strapped to the tether and dragged along. This limited the operation radius to 150 m. At the surface, both sensors were connected to a PC running the sensors' software MSDA_xe (TriOS, Rastede, Germany) for triggering and recording. An additional irradiance sensor (type SAMIP) was mounted on a tripod 1.5 m above the sea-ice surface to measure incident solar radiation (E_d). All sensors were triggered synchronously in intervals of 2 to 10 s, depending on light conditions under the ice, resulting in horizontal resolutions between 0.5 and 2.5 m. Integration times of the sensors varied between 512 and 4048 ms and were dependent on ice conditions, with longer times for the irradiance sensor due to the lower light transmittance of the opaque cosine receptor.

2.5 Additional measurements and under-ice positioning

Sea-ice thickness, snow depth, surface layer thickness or pond depth, and freeboard were measured at each marker (Fig. 4). Additional measurements of total sea-ice thickness were performed at most stations by EM31-measurements along the ROV-transects after completing all dives. Furthermore, surface features, such as pond distributions along the profiles, were noted and photographed to support later analyses.

TCD
6, 3613–3646, 2012

Based on all these observations, a meta-data set was generated for each optical measurement (spectrum). In order to assign local x- and y-coordinates to each under-ice measurement, pass-times of the markers were extracted from the video recordings of all dives and positions were linearly interpolated between two markers. All measurements that could not be located due to uncertain dive tracks were discarded for analyses and are not included in the presented data set. However, these data are included in the supplemental data set, which is available online (Nicolaus and Katlein, 2012), because they may be useful for future applications, e.g. in comparison with other ROV or autonomous under-water vehicle (AUV) transects or for more statistical analyses. The accuracy of the measurement position is expected to be better than 1.0 m in all three dimensions. Uncertainties of the horizontal position during depth profiles and deeper horizontal transects are likely larger, but unknown. Measurement depth (z coordinate) was given by the ROV, because this depth was available for all measurements, other than the measurement of the Ramses IP module, which was not available for all $I_{d,u}$ spectra. Constant x-y coordinates are assumed for all depth profiles, since no better information about horizontal displacement is available.

2.6 Spectral data processing

All optical data were recorded as raw data and calibrated as described in Nicolaus et al. (2010b). Afterwards, all spectra were interpolated to a 1-nm grid before calculating ratios from different sensors, in order to account for sensor-dependent wavelength grids. Spectral transmittance $T_E(\lambda)$ was calculated as

$$T_E(\lambda) = E_{Dt}(\lambda)/E_D(\lambda) \quad (1)$$

with wavelength λ. Similar to spectral reflectance (e.g. Perovich, 1996), spectral transflectance

$$T_I(\lambda) = I_{Dt}(\lambda)/E_D(\lambda) \quad (2)$$

TCD
6, 3613–3646, 2012

was introduced for radiance fluxes measured under ice or in open water in relation to surface irradiance. Similarly, PAR transmittance

$$T_{E,\mathrm{PAR}} = \frac{\int_{400}^{700} T_E(\lambda) E_D(\lambda)\,\mathrm{d}\lambda}{\int_{400}^{700} E_D(\lambda)\,\mathrm{d}\lambda} \tag{3}$$

and PAR transflectance

$$T_{I,\mathrm{PAR}} = \frac{\int_{400}^{700} T_I(\lambda) E_D(\lambda)\,\mathrm{d}\lambda}{\int_{400}^{700} E_D(\lambda)\,\mathrm{d}\lambda} \tag{4}$$

were calculated.

In order to increase comparability, all measurements were also corrected to the ice-water interface, subtracting the effect of the water between the ice and the sensor. Irradiance depth profiles were measured at each station and analyzed to obtain the extinction characteristics of the local seawater. To calculate the spectral and PAR extinction coefficients $k(\lambda)$, the data were fitted for each wavelength or broadband value separately with an exponential decay model

$$E_D(\lambda, z) = E_D(\lambda, z_0) \cdot \exp(-k(\lambda) \cdot z) \tag{5}$$

in the upper 8 m of the water column. The resulting correlation coefficient R^2 of the fits was better than 0.9 for all extinction spectra. Corrected fluxes at the ice water interface are then given by

$$E_{Dt\_\mathrm{corrected}}(\lambda) = \frac{E_{Dt\_\mathrm{measured}}(\lambda)}{\exp(-k(\lambda) \cdot d)} \tag{6}$$

where the distance to the ice d is given by the altimeter measurement. During the stations on 22 August and 31 August no irradiance depth profiles could be recorded and extinction characteristics from 19 August and 2 September were used instead.

TCD
6, 3613–3646, 2012

During and after the cruise, all sensors were set-up for comparison measurements in order to obtain uncertainties and relative differences in measured fluxes. These were expected based on earlier experiences for low solar elevation angles due to inaccuracies of the cosine receptor of the irradiance sensors. This inter-comparison revealed differences of up to 5 % with reproducible characteristics of single sensors. Hence, these differences were corrected during data processing by wavelength-independent scaling of measured fluxes.

Another error source that had to be accounted for during data processing was a high noise level on some radiance spectra. These resulted most likely from insufficient grounding of the radiance sensor, which was operated through the extra cable. All fluxes at wavelengths < 350 and > 800 nm were removed. Afterwards, a spectral value was replaced by a 7-point running mean when its value differed from a 3-point running mean by more than 3 %. This method was found to be most efficient in terms of data quality and had the smallest influence on the measured signal itself. As a consequence, upcoming applications will only use sensors operated through the ROV without extra cables.

3 Results

3.1 Advances in methodology

Operation of spectral radiometers on the ROV allowed for the collection of the most comprehensive and so far unique data set of radiation transmission through Arctic sea ice. Most obvious is the good measurement progress and the flexibility to perform horizontal and vertical transects under very different ice conditions. Using the ROV instead of multiple spot measurements allowed most efficient and non-destructive mapping of under ice radiation, covering a large degree of spatial variability at different scales. Accessing the under-ice environment through the ponds on the sea ice was found to be most efficient and convenient, since these provide a sheltered spot with comparably

TCD
6, 3613–3646, 2012

thin (if any) sea ice. Also, only the direct access to the ice allowed gathering all the ice-specific, in particular surface, observations. Balancing the tether and the ROV slightly heavy turned out to be most practical, since no incidents of tether tangling under the sea ice were encountered. The net dive time of the ROV was below 2 h on each ice station, while the entire station time was 6 to 8 h, including all sea-ice and snow observations, and setup. It would not have been possible to gather any similar data sets with spot measurements from the surface or with divers.

The ROV type itself was found to be most adequate for these kinds of measurements. Its dimensions and weight were small enough to be handled by two persons on the ice, including launch and retrieval without further equipment. Also, its thrusters were strong enough to navigate the ROV in the desired direction. Its payload was large enough to carry the two additional sensors, and it would have been large enough to add a few more small sensors. However, using a fiber-optics tether with higher data capacity (e.g. HD video, more sensors) would certainly be an improvement for future fieldwork.

Based on the presented methods, it was possible to map light transmission through different ice conditions. In addition, the operation from a high-class icebreaker allowed a transpolar transect, observing light penetration into the upper ocean, influenced by Atlantic and Pacific water masses. The measurements were performed during 9 successful ice stations along 51 horizontal profiles with a total length of 4.4 km. In addition, 11 depth profiles, reaching depths > 10 m were recorded. All measurements as well as corresponding surface and ice conditions are summarized in Fig. 4 and Table 1. After processing, the final data set consists of 2900 irradiance and 6400 radiance spectra (all geo-referenced and quality controlled) with a mean horizontal resolution of about 1.0 m. In this respect, it was also found to be most beneficial, to include a variety of ROV-internal measurements (distance to ice, depths, ROV attitude) into the data set. Together with the surface observations, this multi-sensor approach is likely most beneficial to a variety of interdisciplinary applications, and can easily be extended with more sensor types on the ROV. The final data set of all spectra and metadata contains all

TCD
6, 3613–3646, 2012

fields summarized in Table 2. This data set is available online through the Pangaea data publishing and archiving system (www.pangaea.de, Nicolaus and Katlein, 2012).

Another new and most beneficial aspect was to operate one radiance and one irradiance sensor synchronously. Measurement frequency was set as high as possible for both sensors in order to obtain the highest spatial resolution. Over all, the sampling rate of the radiance sensor was higher than that of the irradiance sensor due to shorter integration times. These synchronous measurements were done at all stations, except on 22 August when the irradiance sensor did not work due to a break in the tether cable. With this concept, both, spatial variability and energy budgets, were quantified along identical transects. It was found that it is not possible, as it might be expected for an entirely isotropic light field, to scale measured radiance with a factor of π (= 3.1415) to obtain irradiance. This points to the fact that the light field under sea ice is not isotropic. Finally, this was one reason to introduce transflectance to relate under-ice radiance with surface irradiance (Eq. 2).

3.2 Transmission through sea ice

Figure 6 shows frequency distributions of total transmittance and total transflectance for each of the 9 ice stations. Modes of the frequency distributions mostly represent the difference between white ice and melt ponds. Comparing both plots for each station, characteristic differences become obvious. (1) Modes of transflectance are more pronounced than for transmittance, representing the different characteristics of the radiance and the irradiance sensors. (2) White ice modes of transflectance range up to 0.03 and are lower than those for melt ponds, ranging from 0.08 to 0.16. Only modes for open water were found to be higher (station on 17 September). (3) The distribution functions of transflectance show that the spatial variability of light transmission through sea ice ranges over more than one order of magnitude for all stations. (4) Including the meta data of each ice station (Table 1), it can be shown that light transflectance is generally lower for MYI than for FYI.

TCD
6, 3613–3646, 2012

Exact numbers of all these findings strongly vary from station to station. This is because light transmission depends not only on ice types (FYI, MYI, new ice), but in particular also on surface conditions (scattering layer, snow cover, wet and frozen surfaces) and ice properties (thickness and texture). Merging all data, the frequency distribution for the entire expedition (not shown here) does not reveal as clear modes. This is mostly because surface conditions changed during the cruise and an increasing snow cover towards the end of the cruise reduced light transmission, resulting in a shift of the modes towards lower values. This shows that the spatial heterogeneity is strongly influenced by seasonal (temporal) variability.

3.3 Repeated transects at different depths

Exemplary for all the transects, collected during this study, Fig. 7 shows the results of transflectance measurements under snow-covered FYI and a refrozen lead (new ice) on 9 September. During this station, repeated transects were performed along the same profile at depths of 1.0 m, 2.0 m (twice), and 4.0 m. The aim of these repetitions was to compare the data quality from different depths as well as to estimate errors of this methodology resulting from uncertainties in the under-ice positioning. The geometry of snow and sea ice as measured and interpolated from manual drillings is shown in Fig. 7a. Sea-ice thickness ranged from 0.12 to 1.58 m, snow depth from 0.00 to 0.18 m, and freeboard from 0.01 to 0.49 m. Over all thickness measurements, it was found that sea-ice draft readings obtained from drillings and the ROV matched sufficiently well. Hence these values may also be used for further studies, e.g. to include sea-ice thickness into light-transmission parameterizations.

The differences in total transflectance of the two dives at 2.0 m depth (Fig. 7b), illustrate the combined effect of the high variability on small scales due to the fact that not exactly the identical profile was flown, and that sampling along the line was not at the exact same position. Lateral and along-profile shifts affect measured transmittances due to changing ice conditions above the sensor. However, both dives show the same pattern of higher light transmission through the thinner new ice than the FYI. Also, the

TCD
6, 3613–3646, 2012

total transflectance of 0.04 to 0.06 of both dives under the thin ice agrees very well. In addition, there is good agreement in local increases of transflectance along the profile.

The dives at 1.0 and 4.0 m depths show the same pattern as at 2.0 m with the expected higher (at 1.0 m) and lower (at 4.0 m) transflectances (Fig. 7c). But due to the strong impact of the snow cover, the results show, that it is not possible to find any linear or exponential relation between the measured tranflectances and ice thickness or dive depth. The dive at 1.0 m, almost directly at the sea-ice bottom, also represents sea-ice and snow geometry in high detail. Comparing this to the dive at 4.0 m, shows the effect of proximity to the ice for the measurements, since most geometric features of the FYI, as well as variability in the new ice, are strongly dampened, if visible at all. It was also found that deeper transects were more difficult to correlate to surface properties, because the positioning error was larger due to different view angles, impacting the passing times of the under-ice markers.

4 Discussion

4.1 Methodological advancements

Under-ice radiation measurements with ROVs make use of advancements in sensor and ROV technologies. This allows comprehensive studies that were not possible until a few years ago. With the ROV, it was possible to access the difficult and highly heterogeneous under-ice environment and to map radiation through combined horizontal and vertical transects in a few hours at floe-scales (up to 300 m). Larger areal coverage is also possible, using longer tether cables or re-positioning the access hole on the same ice floe. Another option is to operate the ROV directly from the vessel, as it might be most useful in marginal ice zones or under thin and new sea ice. However, only operating it from ice floes, which were accessible for additional measurements, allowed the acquisition of complementary data sets of sea-ice and snow properties.

TCD
6, 3613–3646, 2012

The resulting multi-sensor data set of several thousand spectra with coincident sea-ice and snow observations also allows new approaches in terms of data analyses, such as the use of frequency distributions to derive representative modes for different ice conditions and to describe horizontal and vertical variability. Based on these presented, but very general findings, more analyses has to be done. However, these facts already underline the value of such comprehensive data sets and this description indicates how such data sets will likely improve our understanding of the differences in radiation transfer through the heterogeneous sea ice. Hence, such measurements and data sets could be used to compare FYI and MYI or ponded and white ice, as well as to improve the description of seasonality. Publishing the presented data set online (Nicolaus and Katlein, 2012) also makes the data immediately available for further analyses and comparisons with other observations, model results, and assumptions. One approach could be to derive new parameterizations for the light transfer through sea ice in numerical models. It could also be possible to derive a measure of uncertainty and variability for previous (point) measurements (e.g. Nicolaus et al., 2010a; Light et al., 2008), e.g. including additional information on sea-ice and snow conditions.

The presented method is almost non-destructive. In future applications, this will also allow repeated transects during different seasons/ice conditions. This is of particular interest, since the understanding of under-ice radiation is still rather poor and only few data exist, combining time series with aspects of spatial variability. Another aspect of the presented approach is that it reduces the need of frequent drillings into the ice, minimizing effects on sea-ice hydrography like artificial surface drainage, particularly during summer (Eicken et al., 2004; Polashenski et al., 2012).

4.2 Multi-sensor approach

Synchronous measurements of spectral radiance and irradiance turned out to be most complementary and useful. Due to their different field of view, radiance (and transflectance) results may be well used to describe the spatial variability of under-ice light conditions, while irradiance measurements are best suited to describe the total amount

TCD
6, 3613–3646, 2012

of available (short-wave) energy beneath sea ice. Especially the radiance measurements resulted in well-defined modal distributions of radiation under sea ice that may be assigned to different surface types and ice conditions. Comprehensive data sets of under-ice radiation budgets could, e.g. contribute to improve our understanding of radiation transfer through sea ice, especially when combined with surface albedo measurements, such that resulting in-ice absorption may be derived. But in general, more analyses of the presented data and additional observations of similar kinds are needed.

Besides the optical data, particularly measurements of sea-ice draft are most valuable since transects of sea-ice draft are still sparse. In connection with the radiation measurements, sea-ice thickness is highly important, since it may be expected that new correlations between ice-thickness and radiative transfer relations could contribute to a better understanding of the energy and light budget of the upper ocean. Here we combined the autonomous measurements from the altimeter on the ROV with drillings and EM31 data. This was found to be most valuable in order to derive sea-ice thickness along the profiles. Future applications could include additional sensors on the ROV in order to relate those to the optical measurements. In particular CTD, fluorescence, oxygen, and/or nutrient measurements could help to study the connections of physical and biological processes in and under sea ice.

4.3 Uncertainties

The greatest uncertainty in the data set was found to be the horizontal positioning, since most positions had to be interpolated between the under-ice markers. However, due to the large amount of data and statistical methods, it may be assumed that this positioning error does not affect the general conclusions. These effects will mostly average-out when comparing entire stations or averaging over different sea-ice properties. The use of an under water (under ice) positioning system, e.g. Ultra Short Base-Line (USBL), would certainly reduce the time-consuming work to mark the transects and be more efficient in data post-processing. Furthermore, this would give more freedom in transect planning and allow more flexibility in measurements, though surface

TCD
6, 3613–3646, 2012

properties must still be acquired manually along the profiles. In addition, it would most likely increase the accuracy of positioning, although we are not aware what the accuracy under ice will be and how pressure ridges would affect the positioning, since the transponders require a straight line of sight.

Additional sensor inter-comparisons showed deviations between single radiometers of up to 5 %. These differences were corrected during data processing, but only over the entire spectrum. It was not possible to include spectral differences. Therefore, only total transmittances and reflectances are discussed here, without focusing on the spectral variability under sea ice. From all data, fluxes and transmittance/transflectance at the ice bottom were also calculated in order to quantify and later parameterize fluxes into the ocean. This calculation (Eq. 6) uses the depth of the ROV, sea-ice draft from the ROV, and the measured flux at a given depth and the surface. As a consequence, these numbers (Nicolaus and Katlein, 2012) combine uncertainties from all three sensors, which is particularly difficult for rough ice.

4.4 Transfer to other studies

Here we present and discuss the application and results from Arctic summer sea ice only. But the same method, instrumentation, and observation strategy can be used in other seasons and sea ice regions in a very similar way. Depending on ice conditions, the main difference would be the under-ice access, which would demand manmade holes if no melt ponds are present. For thin or new ice, as well as marginal ice zones ice and broken ice, the ROV can also be launched and operated from the vessel. With harsher conditions, the operation of the ROV and the work for all complementary measurements will most likely be more time consuming. Depending on weather conditions (mostly temperature) a more solid and better heated control stand would be needed in addition. Under low solar surface irradiances, as during low-light seasons or around the daily solar minimum, the light conditions under sea ice have to be considered for station planning in order to receive high quality data (signal-noise ratios). During this

TCD
6, 3613–3646, 2012

work, most measurements could be performed around highest solar elevations (except on 11 September).

Here we only present summer data with wide-spread melt-pond coverage and almost no snow cover. This means that transmission is larger than during all other seasons and under-ice fluxes are also among the highest (Nicolaus et al., 2010a). As a consequence, measured under-ice fluxes were large enough to gather high quality data and integration times were not too long. Only on 11 September, when the measurements had to be performed during very low solar elevation angles, the sensor threshold of about 0.3 $W m^{-2}$ was often not reached under sea ice, therefore only few data could be used. Transferring this to surface irradiances, some 10 to 30 $W m^{-2}$ are necessary to perform such under-ice measurements with Ramses radiometers. However, this value would significantly increase with decreasing transmittance, e.g. through snow covers or thicker sea ice.

When transferring these data to other studies, it has to be considered that all presented observations were restricted to the wavelength range from 320 to 950 nm, representing about 80 % of short-wave radiation (250–2500 nm). Since transmittances above 950 nm are negligible and those below 350 nm are also comparably small, this means that presented transflectances and transmittances are larger than for integrals over the short-wave range here. Values for the complete short-wave range can be obtained by scaling the presented data set, using reference spectra (e.g. Grenfell and Perovich, 1984).

The example of repeated dives at different depths down to 4.0 m demonstrates the information loss with increasing depth. This can be compensated to a certain degree with a more narrow field of view (radiance sensors) and higher measurement frequency (if technically possible). This has to be considered when planning such measurements from AUVs in order to get even larger spatial coverage and more wide-spread data. In addition, a larger distance to the ice increases the need for high-quality corrections of the signal towards the ice-ocean interface. This is, as discussed above, one of the greatest uncertainties in this data set.

TCD
6, 3613–3646, 2012

Besides physical studies and general energy-budget estimates, biological applications could make use of this kind of under-ice light measurement system in order to obtain total amount of biomass in and under sea ice. These studies would be based on the spectral information from the data set with the aim of deriving patterns that can be correlated, e.g. to Chlorophyll *a* (Chl *a*) concentrations (Mundy et al., 2007), a proxy for biomass. So far, gathering these data is highly labor intensive and time consuming. In addition, these methods are usually limited to spot measurements or vertical profiles from water samples.

5 Conclusions

Operating spectral radiometers on a ROV was found to be most efficient to map under-ice light (solar short-wave radiation) conditions under Arctic sea ice. The presented measurements were very successful and resulted in a unique data set, describing the spatial (horizontal and vertical) variability of radiative fluxes through sea ice as well as the spectral transmittance and transflectance of summer sea ice. The measurements were the first of its kind and cover a broad range of summer sea-ice conditions, particularly describing differences between ponded and white ice, as well as FYI and MYI. The use of synchronous measurements with spectral radiance and irradiance sensors allowed combined studies of spatial (horizontal and vertical) variability with energy-budget estimates. Combining all these optical measurements with coincident measurements of surface and ice properties can contribute to improve current parameterizations of light transmission through sea ice in numerical models. Performing more similar observations in the coming years, in particular also covering very different sea-ice conditions (seasons and regions), would then contribute to increase our understanding of the large-scale energy-budget of ice-covered oceans.

TCD
6, 3613–3646, 2012

Acknowledgements. We strongly acknowledge the support of the captain, the crew, and the scientific cruise leader Ursula Schauer of R/V *Polarstern* the cruise ARK-XXVI/3, facilitating the presented measurements. Stefan Hendricks, Mario Hoppmann, Priska Hunkeler, and Robert Ricker contributed significantly to succeeding the field measurements. We are most grateful to Werner Dimmler for his technical support on *Polarstern*, as well as the technical support by Ocean Modules, Sweden. This study was funded through the Alfred Wegener Institute for Polar and Marine Research.

References

Arrigo, K. R., Perovich, D. K., Pickart, R. S., Brown, Z. W., van Dijken, G. L., Lowry, K. E., Mills, M. M., Palmer, M. A., Balch, W. M., Bahr, F., Bates, N. R., Benitez-Nelson, C., Bowler, B., Brownlee, E., Ehn, J. K., Frey, K. E., Garley, R., Laney, S. R., Lubelczyk, L., Mathis, J., Matsuoka, A., Mitchell, B. G., Moore, G. W. K., Ortega-Retuerta, E., Pal, S., Polashenski, C. M., Reynolds, R. A., Schieber, B., Sosik, H. M., Stephens, M., and Swift, J. H.: Massive phytoplankton blooms under arctic sea ice, Science, 336, 1408–1408, doi:10.1126/science.1215065, 2012.

Deal, C., Jin, M. B., Elliott, S., Hunke, E., Maltrud, M., and Jeffery, N.: Large-scale modeling of primary production and ice algal biomass within arctic sea ice in 1992, J. Geophys. Res.-Oceans, 116, C07004, doi:10.1029/2010jc006409, 2011.

Ehn, J. K., Mundy, C. J., Barber, D. G., Hop, H., Rossnagel, A., and Stewart, J.: Impact of horizontal spreading on light propagation in melt pond covered seasonal sea ice in the Canadian Arctic, J. Geophys. Res.-Oceans, 116, C00g02, doi:10.1029/2010jc006908, 2011.

Eicken, H., Grenfell, T. C., Perovich, D. K., Richter-Menge, J. A., and Frey, K.: Hydraulic controls of summer Arctic pack ice albedo, J. Geophys. Res., 109, C08007, doi:10.1029/2003JC001989, 2004.

Ficek, D., Kaczmarek, S., Ston-Egiert, J., Wozniak, B., Majchrowski, R., and Dera, J.: Spectra of light absorption by phytoplankton pigments in the Baltic; conclusions to be drawn from a Gaussian analysis of empirical data, Oceanologia, 46, 533–555, 2004.

Frey, K. E., Perovich, D. K., and Light, B.: The spatial distribution of solar radiation under a melting Arctic sea ice cover, Geophys. Res. Lett., 38, L22501, doi:10.1029/2011gl049421, 2011.

TCD
6, 3613–3646, 2012

Grenfell, T. C. and Perovich, D. K.: Spectral albedos of sea ice and incident solar irradiance in the southern Beaufort Sea, J. Geophys. Res., 89, 3573–3580, 1984.
Grenfell, T. C., Light, B., and Perovich, D. K.: Spectral transmission and implications for the partitioning of shortwave radiation in arctic sea ice, Ann. Glaciol., 44, 1–6, 2006.
Light, B., Grenfell, T. C., and Perovich, D. K.: Transmission and absorption of solar radiation by Arctic sea ice during the melt season, J. Geophys. Res., 113, C03023, doi:10.1029/2006JC003977, 2008.
Mundy, C. J., Barber, D. G., and Michel, C.: Variability of snow and ice thermal, physical and optical properties pertinent to sea ice algae biomass during spring, J. Marine Syst., 58, 107–120, 2005.
Mundy, C. J., Ehn, J. K., Barber, D. G., and Michel, C.: Influence of snow cover and algae on the spectral dependence of transmitted irradiance through Arctic landfast first-year sea ice, J. Geophys. Res., 112, C03007, doi:10.1029/2006JC003683, 2007.
Nicolaus, M., Gerland, S., Hudson, S. R., Hanson, S., Haapala, J., and Perovich, D. K.: Seasonality of spectral albedo and transmissivity as observed in the Arctic Transpolar Drift in 2007, J. Geophys. Res., 115, C11011, doi:10.1029/2009JC006074, 2010a.
Nicolaus, M., Hudson, S. R., Gerland, S., and Munderloh, K.: A modern concept for autonomous and continuous measurements of spectral albedo and transmittance of sea ice, Cold Reg. Sci. Technol., 62, 14–28, 2010b.
Nicolaus, M., Petrich, C., Hudson, S. R., and Granskog, M. A.: Variability of light transmission through arctic sea ice during spring, Ann. Glaciol., in review, 2012.
Perovich, D. K.: Theoretical estimates of light reflection and transmission by spatially complex and temporally varying sea ice covers, J. Geophys. Res.-Oceans, 95, 9557–9567, 1990.
Perovich, D. K.: The optical properties of sea ice, Cold Regions Research and Engeneering Laboratory Monograph, 96–1, 24 pages, U.S. Army Cold Regions Research and Engineering Laboratory, Hanover, NH, USA, 1996.
Perovich, D. K.: On the aggregate-scale partitioning of solar radiation in Arctic sea ice during the Surface Heat Budget of the Arctic Ocean (SHEBA) field experiment, J. Geophys. Res., 110, C03002, doi:10.1029/2004JC002512, 2005.
Perovich, D. K., Cota, G. F., Maykut, G. A., and Grenfell, T. C.: Bio-optical observations of first-year arctic sea ice, Geophys. Res. Lett., 20, 1059–1062, 1993.
Perovich, D. K., Roesler, C. S., and Pegau, W. S.: Variability in Arctic sea ice optical properties, J. Geophys. Res.-Oceans, 103, 1193–1208, 1998.

TCD
6, 3613–3646, 2012

Polashenski, C., Perovich, D., and Courville, Z.: The mechanisms of sea ice melt pond formation and evolution, J. Geophys. Res.-Oceans, 117, C01001, doi:10.1029/2011jc007231, 2012.
Popova, E. E., Yool, A., Coward, A. C., Dupont, F., Deal, C., Elliott, S., Hunke, E., Jin, M. B., Steele, M., and Zhang, J. L.: What controls primary production in the Arctic Ocean? Results from an intercomparison of five general circulation models with biogeochemistry, J. Geophys. Res.-Oceans, 117, C00D12, doi:10.1029/2011jc007112, 2012.
Sturm, M. and Massom, R. A.: Snow and sea ice, in: Sea ice, 2nd edn., edited by: Thomas, D. N. and Dieckmann, G. S., Wiley-Blackwell, Chichester, 153–204, 2009.
Warren, S. G., Rigor, I. G., Untersteiner, N., Radionov, V. F., Bryazgin, N. N., Aleksandrov, Y. I., and Colony, R.: Snow depth on Arctic sea ice, J. Climate, 12, 1814–1829, 1999.

TCD
6, 3613–3646, 2012

Table 1. All ROV transects that are included in the final data set. Dates (UTC) refer to the ROV measurements (not necessarily the station beginning). Markers are named with "M" and their number, e.g. M6 for marker number 6. The station number gives the official R/V *Polarstern* station number as reference for any other observations during the cruise. Abbreviations: MYI: multi-year sea ice, FYI: first-year sea ice.

Date Station	Profile (@ ROV depth)	Length/ Depth (m)	Sea ice and thickness	Surface conditions Pond status	Comments
17.08.11	Profile @ 2.5 m	100	FYI 1.1 m	No snow,	
78–209	Profile @ 5.0 m	50	FYI 1.1 m	open ponds	
	Profile @ ice bottom	30	FYI 1.1 m		"Stop and go" mode
	Profile @ ice bottom	no data	FYI 1.1 m		Continuous, bad positioning
	Depth @ M30	50	FYI 1.1 m		
	Depth	13	Open water		
19.08.11	Profile 000° @1.5 m	120	FYI 1.2 m	No snow,	
78–212	Profile 045°, @1.5 m	60	FYI 1.2 m	open ponds	
	Profile 095°, @1.5 m	120	FYI 1.2 m		
	Profile 175°, @1.5 m	120	FYI 1.2 m		
	Profile 220°, @1.5 m	150	FYI 1.2 m		
	Profile ridges, @15 m	points	MYI < 8.0 m		
	Grid @1.5 m	30 × 15	FYI 1.2 m		
	Depth @ M30	50	FYI 1.2 m		
22.08.11	Grid @ variable depth	30 × 50	MYI 1.5–3.5 m	Frozen surface and	Only radiance sensor
78–218	Depth @ M16	10	MYI 1.5–3.5 m	ponds, no snow	
03.09.11	Profile 1 @ 4–8 m	2 × 130	MYI 2.0–3.8 m	2–3 cm new snow,	
78–235	Profile 1 @ 8 m	2 × 130	MYI 2.0–3.8 m	ponds frozen	
	Profile 1 @ variable depth	120	MYI 2.0–3.8 m	(10 cm)	
	Profile 2 @ 2 m	2 × 80	FYI 1.2 m		
	Depth @ M4	90	MYI close FYI		
	Depth @ M8	100	FYI close water		
	Surface depth profile	5	MYI/FYI		

TCD
6, 3613–3646, 2012

Table 1. Continued.

Date Station	Profile (@ ROV depth)	Length/ Depth (m)	Sea ice and thickness	Surface conditions Pond status	Comments
06.09.11 78–238	Profile @ 1.2 m	30	FYI 0.8 m	Snow 3 cm, ponds frozen	
	Profile @ 2.0 m	120	FYI 0.8 (to 2.0)		
	Profile @ 4.0 m	120	FYI 0.8 (to 2.0)		
	Profile @ 6.0 m	105	FYI 0.8 (to 2.0)		
	Profile @ variable depth	120	FYI 0.8 (to 2.0)		
	Cross profile @ 3.0 m	70	FYI 0.8		Bad positioning
	Depth @ M2	50	FYI 0.8 (to 2.0)		
	Depth	5	FYI 0.8 (to 2.0)		
09.09.11 78–245	Profile @ 1.0 m	120	FYI 1.2 m	Snow 10 cm, ponds frozen	
	Profile @ 1.2 m	90	New ice 0.3 m		New ice = frozen lead
	Profile @ 2.0 m	2 × 210	FYI + new ice		
	Profile @ 4.0 m	210	FYI + new ice		
	Profile @ 1.0 m no snow	15	New ice 0.3 m		Snow removed M8-M9
	Profile @ 2.0 m no snow	15	New ice 0.3 m		Snow removed M8-M9
	Profile @ 2.0 m no snow	15	FYI 1.2 m		Snow removed M1-M2
	Depth @ M2	40	New ice 0.3 m		
	Depth @ M11	25	FYI 1.2 m		
11.09.11 78–250	Profile @ 2.0 m	Ca. 4 × 30	New ice + MYI	Ponds frozen, snow covered	Low light level, bad data quality (night station), Bad positioning
	Depth	10	Open water		
	Depth	3	Open water		
16.09.11 78–267	Profile @ 4.0 m	Total 450	MYI 1.7 to 2.9 m	Ponds frozen, snow covered	
	Profile @ variable depth	Total 240	MYI 1.7 to 2.9 m		
	Depth @ M4	50	MYI 1.7 to 2.9 m		
	Depth	25	Open water		

TCD
6, 3613–3646, 2012

Table 2. Variables and dimensions of the master data set as presented in this manuscript and published in the Pangaea data publishing system (Nicolaus and Katlein, 2012).

Variable	Symbol	Unit	Comment
Radiation data			
Irradiance, incident (spectral)	E_D	$\mathrm{W\,m^{-2}\,nm^{-1}}$	
Irradiance, incident (PAR)	$E_{D\mathrm{par}}$	$\mathrm{W\,m^{-2}}$	
Irradiance, transmitted (spectral)	E_T	$\mathrm{W\,m^{-2}\,nm^{-1}}$	
Irradiance, transmitted (PAR)	$E_{T\mathrm{par}}$	$\mathrm{W\,m^{-2}}$	
Radiance, incident (spectral)	I_D	$\mathrm{W\,m^{-2}\,nm^{-1}}$	
Radiance, incident (PAR)	$I_{D\mathrm{par}}$	$\mathrm{W\,m^{-2}}$	
Transmittance (spectral)	T_E		see Eq. (1)
Transmittance (PAR)	$T_{E\mathrm{par}}$		see Eq. (3)
Transflectance (spectral)	T_I		see Eq. (2)
Transflectance (PAR)	$T_{I\mathrm{par}}$		see Eq. (4)
Meta data			
Date/Time	t	String	
x-coordinate	x	m	
y-coordinate	y	m	
z-coordinate = depth	z	m	
Sea-ice thickness	z_i	m	
Snow depth	z_s	m	
Freeboard	fb	m	

TCD
6, 3613–3646, 2012

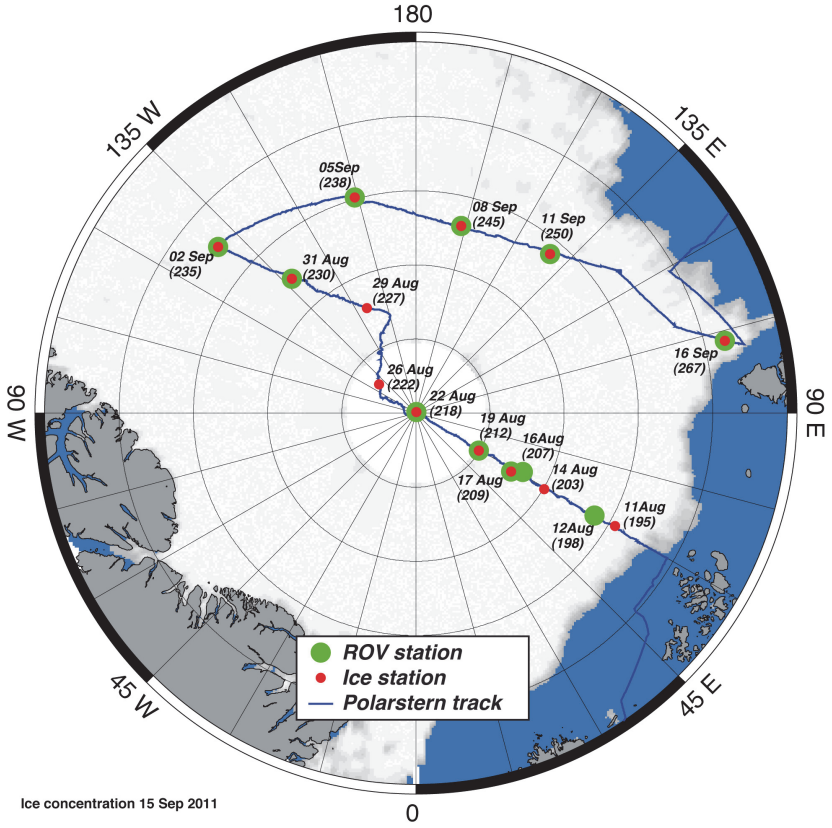

Fig. 1. Ice stations and ROV stations during R/V *Polarstern* cruise ARK-XXVI/3 (TransArc 2011). The background image gives sea-ice concentration on 15 September 2011 (from: http://iup.physik.uni-bremen.de). The Magnetic Pole was close to the ice station on 31 August 2011.

TCD
6, 3613–3646, 2012

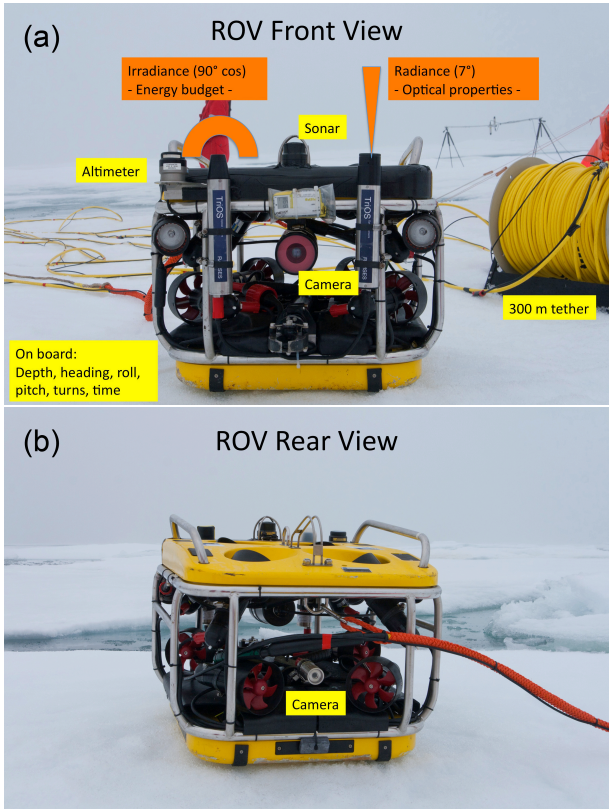

Fig. 2. Annotated photographs of the ROV equipped with sensors for under-ice radiation measurements. **(a)** Front view including the two Ramses radiometers, one measuring irradiance (left) and one measuring radiance (right). Surface sensors are shown in the back, too. **(b)** Rear view with tether.

TCD
6, 3613–3646, 2012

Fig. 3. Photograph of the ROV site taken from board during the ice station on 2 September 2011. The main picture shows the deployment hole in a frozen melt pond (pond-ice thickness: 5 cm), the yellow tether, and the pilot tent. The inset picture shows two ROV pilots, one controlling the ROV and one controlling the sensors and documenting all operations.

TCD
6, 3613–3646, 2012

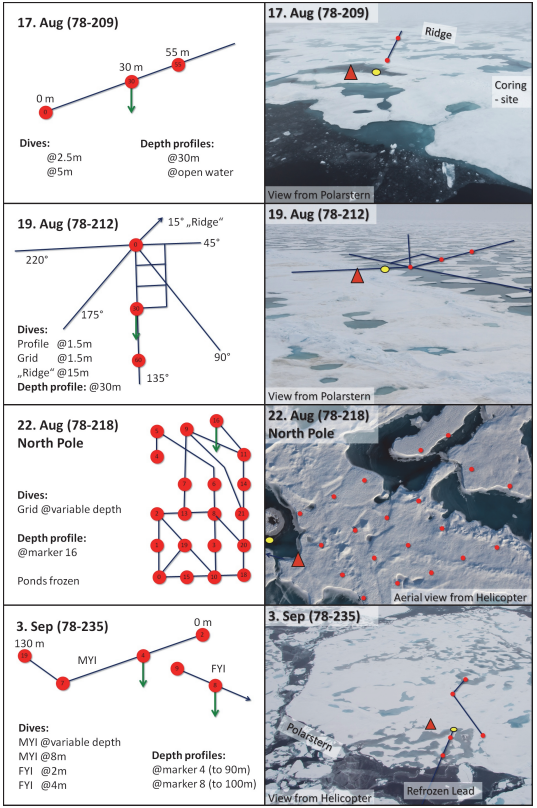

Fig. 4a. Sketches and Overview images of ROV sea-ice stations with profile lines (dark blue), selected markers with according numbers (red dots), depth profiles (green arrows), bio-optical cores (light green cylinders), and the depths of main dives. The yellow ellipse indicates the ROV launch hole and the red triangle the location of the pilot tent.

TCD
6, 3613–3646, 2012

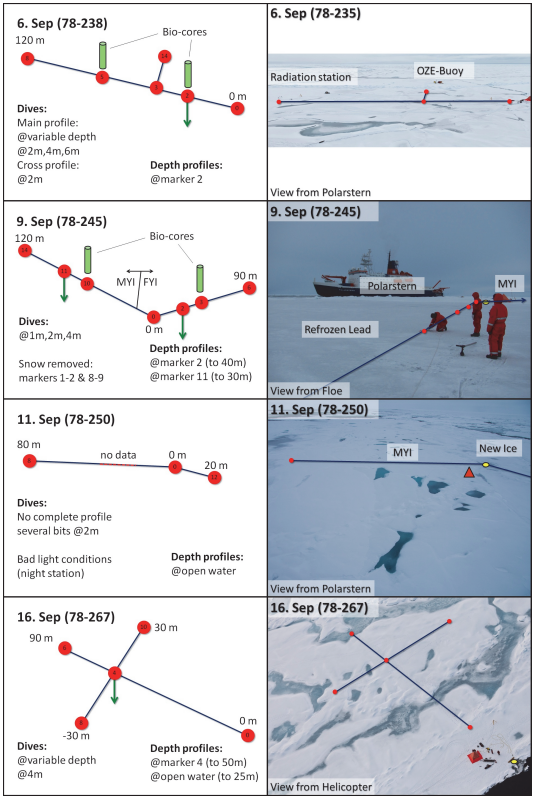

Fig. 4b. Sketches and Overview images of ROV sea-ice stations with profile lines (dark blue), selected markers with according numbers (red dots), depth profiles (green arrows), bio-optical cores (light green cylinders), and the depths of main dives. The yellow ellipse indicates the ROV launch hole and the red triangle the location of the pilot tent.

TCD
6, 3613–3646, 2012

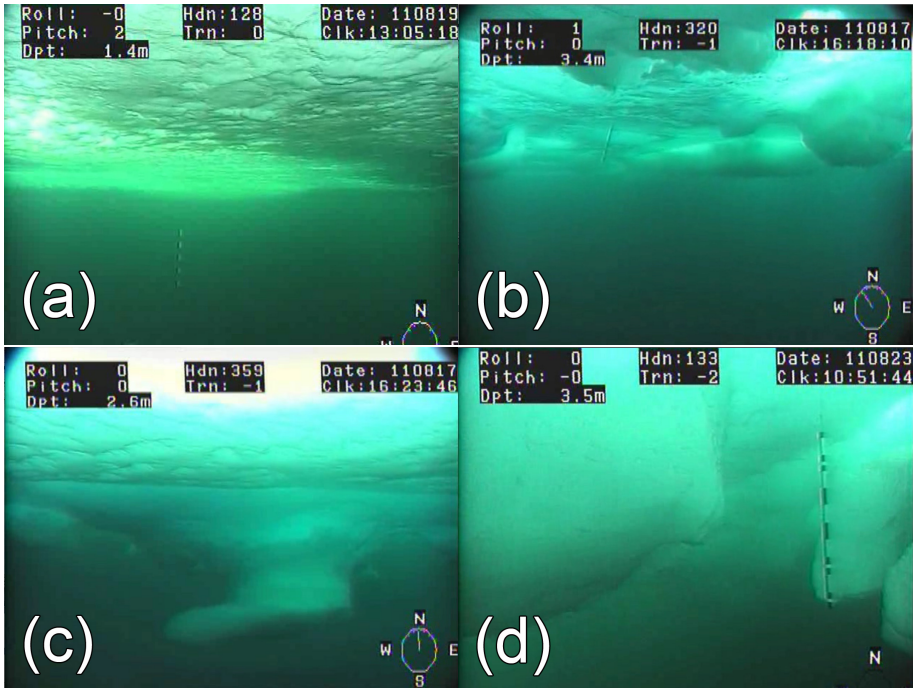

Fig. 5. Impressions of light conditions under sea ice. Photographs are stills of the ROV front camera video. **(a)** Level ice with a melt pond at the marker position **(b)** Patches of level and ridged ice with high variability in light conditions **(c)** Ponded ice in front (bright) and ridged ice (darker) in the back **(d)** Ridged sea ice. The markers (visible in **a**, **b**, and **d**) are 1.0 m long. Binary coding of the marker in **d** identifies it as number 19 (IOOII, white marks on the red sections read from bottom up). Overlays give dive information: Roll, pitch, depth, heading, turns, date (format: yymmdd), time (UTC), and a compass rosette.

TCD
6, 3613–3646, 2012

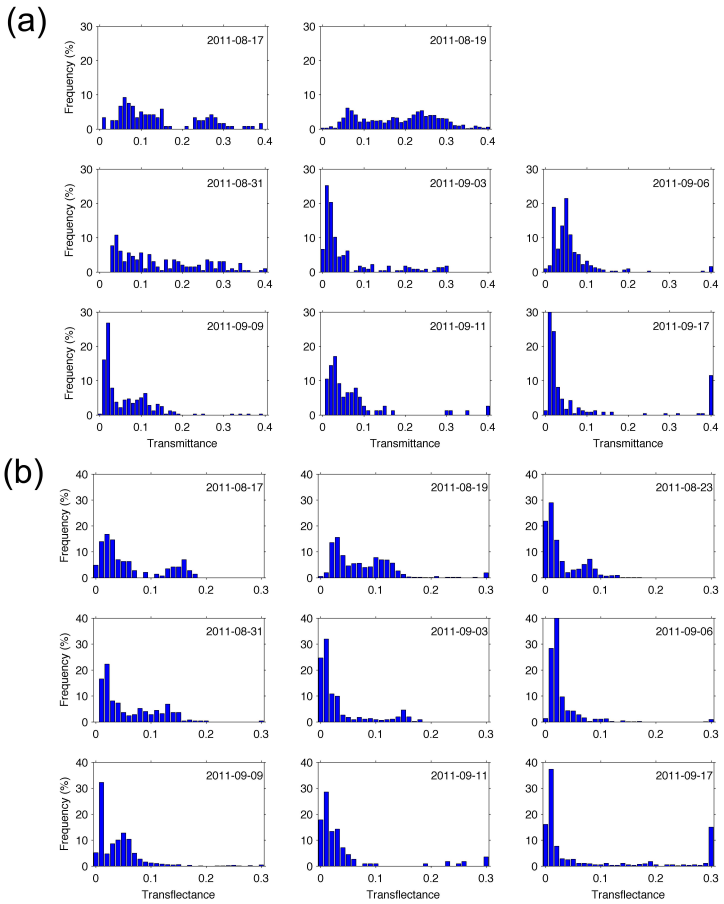

Fig. 6. (a) Transmittance and **(b)** transflectance of all measurements for each station. All bins are 0.01 wide. No transmittance measurements on 23 August.

TCD
6, 3613–3646, 2012

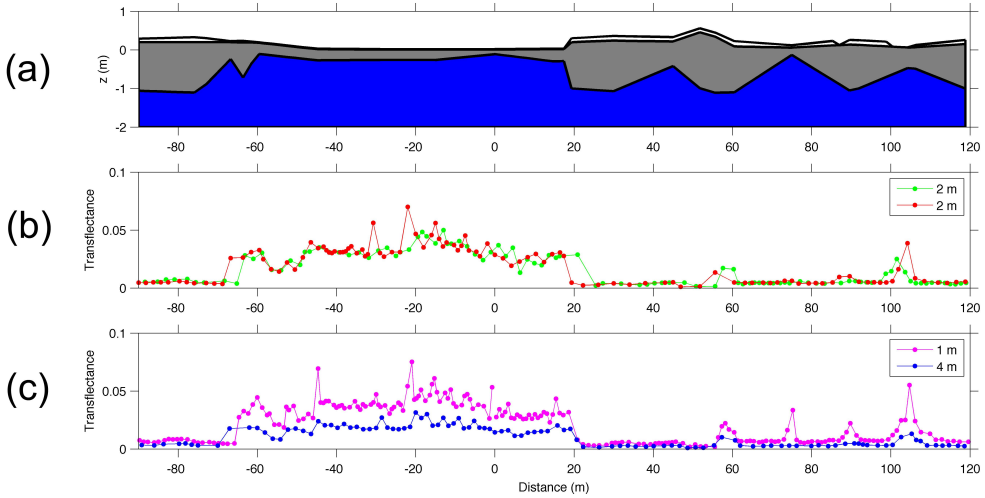

Fig. 7. Transflectance measurements in different depths along a profile of old sea-ice and a refrozen lead ($-65 < x < 20$ m) on 9 September 2011. **(a)** Profile geometry of snow depth, freeboard, and sea-ice draft from drillings. **(b)** Transflectance measured during 2 dives in the same depth of 2 m. **(c)** Transflectance measured at 1.0 and 4.0 m depth. X-axis nomenclature is according to the field settings with the access hole at $x = 0$ m (Fig. 4b).

TCD
6, 3613–3646, 2012